Adaptive Guidance for an Aero-Assisted Boost Vehicle

Bandu N. Pamadi
Vigyan Research Associates, Inc., Hampton, Virginia 23666-1325
and
Lawrence W. Taylor Jr. and Douglas B. Price
NASA Langley Research Center, Hampton, Virginia 23665-5225

An adaptive guidance system incorporating a dynamic pressure constraint is developed for a single stage to low Earth orbit, with thrust gimbal angle as the control variable. The ascent profile is represented in the form of a two-segment cubic spline function whose parameters are optimized for maximum payload. The flight to low Earth orbit is divided into initial and terminal phases. In the initial phase, a fully adaptive scheme is used wherein a new ascent profile is generated for the remainder of flight whenever the simulated vehicle deviates beyond a prescribed limit. In the terminal phase, a semiadaptive scheme with a linear feedback control is used to keep the vehicle close to the nominal path. This two-phase adaptive guidance algorithm is applied to a generic aero-assisted booster.

Nomenclature

a,b,c,d = coefficients of cubic spline, Eq. (8)
C_L = lift coefficient
C_i^j = direction cosine matrix for transformation from system i to system j
D = aerodynamic drag
F = force vector $[F_x,F_y,F_z]^T$
g = gravitational acceleration
h = altitude
h^* = endpoint altitude for initial guidance phase
h_1 = intermediate altitude where the two spline segments are connected
h_{des} = desired altitude as given by spline ascent profile, Eq. (8)
h_a = current altitude of the booster vehicle
h_f = final altitude
K_1,K_2 = feedback gains
L = aerodynamic lift
L_0 = longitude
M = Mach number
m = mass of the boost vehicle
m_0 = initial mass ($t=0$)
m_p = final mass at $h=h_f$
q = dynamic pressure $=\frac{1}{2}\rho V_e^2$
R = position vector
T = thrust
V = current inertial velocity
V_0 = inertial velocity on the surface of Earth
V_f,V_1 = inertial velocity at $h=h_f$ and h_1, respectively
R_{01} = radius vector from Earth's center to origin of $x_ny_nz_n$ system
xyz = rectangular coordinate system

Bandu N. Pamadi is a senior research scientist at Vigyan Research Associates, Hampton, Virginia. He received his Ph.D. in Aeronautical Engineering in 1973 from the Indian Institute of Technology, Bombay. His research interests are in the areas of aerodynamics, flight dynamics, and guidance and control of aerospace vehicles.

Lawrence W. Taylor Jr. is the Chief Scientist of the Guidance and Control Division, NASA Langley Research Center, Hampton, Virginia. His specialties include systems identification, parameter estimation, and optimal control. Applications studied include the X-series research airplanes, lifting body aircraft, and the Space Shuttle.

Douglas B. Price is Head of the Spacecraft Controls Branch of the Guidance and Controls Division at NASA Langley Research Center. He has a Ph.D. in Applied Mathematics from North Carolina State University. He has contributed to the areas of guidance and control for aerospace vehicles, onboard control algorithms for aircraft, analytical redundancy, and generalized functions.

Received July 18, 1988; presented as Paper 88-4173 at the AIAA Guidance, Navigation and Control Conference, Minneapolis, MN, Aug. 15-17, 1988; revision received March 20, 1989.

α = angle of attack
β = coefficient in the exponential atmospheric density model
γ = flight-path angle
δ = semivertex angle of the booster
ϵ = percent error margin ($\Delta h/h$)
λ = geographical latitude
θ_T = thrust gimbal angle
$\theta_{Tmax}, \theta_{Tmin}$ = maximum and minimum limits, respectively, of thrust gimbal angle
Ω = angular velocity of the Earth about its own axis
$( )'$ = differentiation with respect to inertial velocity
$(\dot{})$ = differentiation with respect to time

Subscripts

b = body
e = Earth-related
i = inertial
n = navigational
max = maximum value

Introduction

ONE of the likely candidates actively studied in the Advanced Space Transportation program of NASA is a fully reusable system that is capable of carrying the payloads more efficiently than the system used by the Space Shuttle.[1-3] Such a vehicle delivers its payload to a space station in low Earth orbit (LEO) or to an orbit transfer vehicle at the space station for final delivery to the geosynchronous orbit.

Current boost operations of the Space Shuttle require extensive preparations for the guidance system preceding the launch. An important factor in reducing the cost of operation to boost the payloads to LEO is to be able to "launch on demand." This requires that the guidance law be adaptive and capable of accommodating deviations in predetermined launch conditions, variations in weather, and off-nominal system performance. Simultaneously, the guidance law must be capable of incorporating state constraints like maximum dynamic pressure and aerodynamic heating limits.

In this paper, we address the task of developing an adaptive guidance algorithm with dynamic pressure constraint for an aero-assisted booster to LEO. The guidance algorithm consists of three parts: simulation of vehicle dynamics, derivation of optimal ascent profile, and determination of the control setting, or the guidance law. The vehicle dynamics is simulated by the solution of equations of motion in inertial space considering a rotating spherical Earth with an inverse square gravity field, an empirical aerodynamic model for the vehicle, and an exponential atmospheric model. The control variable is assumed to be the thrust gimbal angle. Various coordinate systems are introduced to derive real-time information on vehicle position and velocity suitable for guidance and navigation. The ascent profile that defines the desired altitude h as a function of inertial velocity is represented by cubic spline functions.[4] A cubic spline is a form of polynomial approximation used to describe the variation of a given function between successive pairs of points. A general cubic spline is a third-degree polynomial involving four constants, which insures continuous differentiability of the function and continuity in first and second derivatives. Here, the trajectory is represented by two cubic spline segments, which are connected at an intermediate altitude designated as h_1 (Fig. 1). The altitude h_1 and the slope h_1' at the junction point of the splines are the two free parameters, which completely define the ascent profile, given the prescribed initial and final conditions. A gradient optimization technique, with payload delivered at the orbit as the cost function, is used to derive the optimal values of h_1 and h_1'.

For guidance law development, the flight of the vehicle to LEO is divided into initial and terminal phases. The initial phase is assumed to extend to a conveniently chosen altitude h^* such that, at altitudes beyond h^*, the vehicle is virtually out of the Earth's atmosphere. The terminal phase extends from h^* to LEO. In the initial phase, a fully adaptive guidance scheme is used; i.e., whenever the vehicle deviates by more than a predetermined margin from the optimal ascent profile, a new optimal spline profile is generated for the remainder of the flight, and the previous one is discarded. This gives new values of h_1 and h_1'. The gimbal angle is then set to fly along the new trajectory. This approach is continued until the vehicle reaches the end point h^* of the first phase. The flight path in the second phase is assumed to consist of a single cubic spline segment, which has only one free parameter h_1', to be determined by gradient optimization as before. This defines the nominal path for terminal phase. A linear, proportional plus derivative feedback control is employed to keep the deviations of the vehicle within acceptable limits from the nominal path until the desired Hohmann transfer orbit is reached.

This guidance algorithm is applied to the flight of an aero-assisted generic rocket booster to LEO.

Simulation of Vehicle Dynamics

The purpose of performing these computations is to simulate the flight of the boost vehicle to LEO. This simulation makes use of four different systems of Cartesian coordinate axes as shown in Figs. 2 and 3. A description of these axes systems and various transformation matrices is given in Appendix A. The simulation consists of the following steps.

Step 1: Solve the equations of motion in an inertial ($x_i y_i z_i$) frame of reference. The gravity, propulsive, aerodynamic, and control forces are to be transformed from their respective frames of reference to the inertial system.

Step 2: Transform the given initial conditions, such as the position and velocity of the booster at launch, to the inertial reference system.

Step 3: Transform the inertial solution to other reference systems to obtain the position, velocity, and acceleration of the

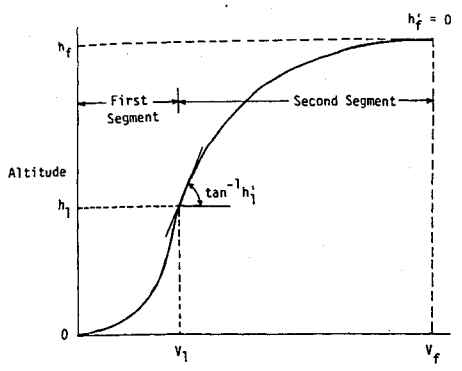

Fig. 1 Ascent profile, two-segment spline function (Ref. 4).

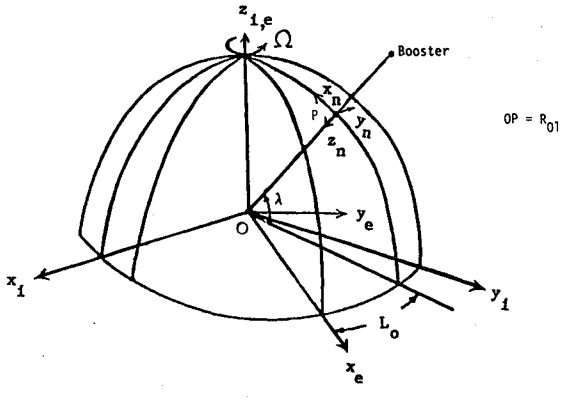

Fig. 2 Coordinate systems.

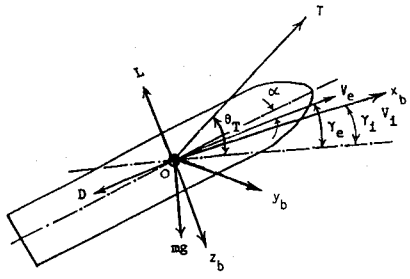

Fig. 3 Forces acting on the booster vehicle.

booster suitable for guidance, navigation, and control purposes.

The equations of motion are,

$$m\ddot{R}_i = F_i \tag{1}$$

where

$$R_i = \begin{bmatrix} x_i \\ y_i \\ z_i \end{bmatrix}, \qquad F_i = \begin{bmatrix} F_{xi} \\ F_{yi} \\ F_{zi} \end{bmatrix} \tag{2}$$

The external force vector F_i consists of gravity, propulsive, aerodynamic, and control forces (Fig. 3). In a body-fixed coordinate system,

$$F_{xb} = T\cos(\theta_T - \gamma_i) - L\sin(\gamma_e - \gamma_i) - D\cos(\gamma_e - \gamma_i) - mg\sin\gamma_i \tag{3}$$

$$F_{yb} = 0 \tag{4}$$

$$F_{zb} = -T\sin(\theta_T - \gamma_i) - L\cos(\gamma_e - \gamma_i) + D\sin(\gamma_e - \gamma_i) + mg\cos\gamma_i \tag{5}$$

so that

$$F_i = C_b^i \begin{bmatrix} F_{xb} \\ F_{yb} \\ F_{zb} \end{bmatrix} \tag{6}$$

Constraint:

$$q \le q_{\max} \tag{7}$$

A successive integration of Eq. (1), using Eqs. (3–6) and subject to constraint (7) gives the velocity and position of the vehicle in inertial space. The position and velocity in other reference systems can be obtained using the relations given in Appendix A. The method of handling the dynamic pressure constraint (7) is discussed later.

Optimal Ascent Profile

The ascent profile is determined by an open-loop optimization procedure. This profile gives the desired variation of altitude with inertial velocity and forms the nominal path for the simulated vehicle. In this paper, this profile is represented in the form of a two-segment cubic spline function (Fig. 1) as follows. Following Ref. 4,

$$h = a + b(V_i - V_0) + c(V_i - V_0)^2 + d(V_i - V_0)^3 \tag{8}$$

where

$$a = h_0 \tag{9}$$

$$b = h_0' \tag{10}$$

$$c = \frac{3(h_f - h_0) - (V_f - V_0)(2h_0' + h_f')}{(V_f - V_0)^2} \tag{11}$$

$$d = \frac{(V_f - V_0)(h_f' + h_0') - 2(h_f - h_0)}{(V_f - V_0)^3} \tag{12}$$

For segment 1, $h_0 = 0$ and $h_0' = 0$. V_0 is the initial velocity at launch, and $V_0 = \Omega R_e \cos\lambda$, for launch starting from rest on the surface of Earth with latitude λ. We assume that launch is to the east to take advantage of Earth's rotation ($\Omega = 0.7272 \times 10^{-4}$ rad/s).

For segment 2, $V_0 = V_1$, $h_0 = h_1$, and $h_0' = h_1'$. The terminal velocity V_f and altitude h_f depend on the parameters of LEO. For circular orbit, $h_f' = 0$.

The value of V_1 is somewhat arbitrary. Here it is chosen as 5500 ft/s. This leaves two more parameters, h_1 and h_1', to be specified so that spline segments 1 and 2 are completely described.

The problem of finding h_1 and h_1' is now formulated as a gradient optimization problem, with h_1 and h_1' as two parameters to be determined such that the payload delivered to the orbit is maximized. In this paper, such a two-segment cubic spline function with optimum values of h_1 and h_1' is referred to as an optimal ascent profile. The details of this analysis are given in Appendix B. This approach, wherein the form of ascent trajectory is prescribed and the parameters of this prescribed trajectory are optimized, is generally inferior to the more rigorous approach based on variational calculus, which usually gives a globally optimal trajectory. However, the present method has an advantage in that it is mathematically simpler and computationally efficient. Only a small number of parameters have to be determined to define an optimal ascent profile. Such a feature is especially desirable for onboard guidance schemes to LEO, where the entire duration of flight is of the order of only a few minutes.

Guidance

The guidance concept evolves from the basic requirement that the vehicle attain the prescribed Hohmann transfer orbit with optimum payload delivery. The control variable postulated is the thrust gimbal angle. The aerodynamic control through angle-of-attack modulation is not considered. The booster flight to LEO is divided into initial and terminal phases. The initial phase extends from the surface of Earth to a conveniently chosen altitude h^*. The terminal phase is assumed to extend from h^* to final altitude h_f. A fully adaptive guidance scheme is used in the initial phase, and a semi-adaptive guidance scheme is used in the terminal phase.

Initial Phase: Fully Adaptive Scheme

At $t = 0$, let the vehicle lift off with the thrust gimbal angle θ_T (determined as explained later) so as to follow the desired initial ascent profile (determined at $t = 0$). However, it may happen that, at $t = t'$, the vehicle altitude h_a is different from the corresponding desired value and may exceed a predetermined error margin ϵ. The reason for these differences are explained later. Now, instead of attempting to return to the desired trajectory, which may involve loss of altitude, a different strategy is adopted. At this time $t = t'$, a new optimal trajectory for the remainder of the flight is generated, with initial conditions corresponding to velocity and altitudes of the vehicle at $t = t'$. This process generates a set of new values for h_1 and h_1'. The previous values of h_1 and h_1' are discarded. A fresh value of gimbal angle (θ_T) is determined using the

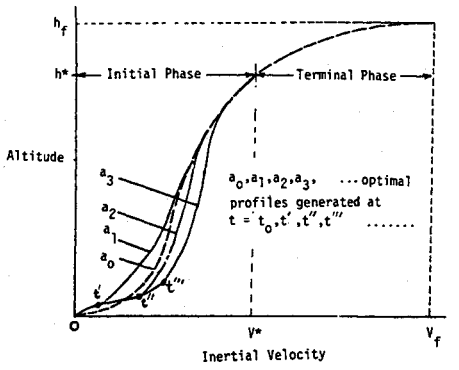

Fig. 4 Schematic illustration of adaptive guidance scheme.

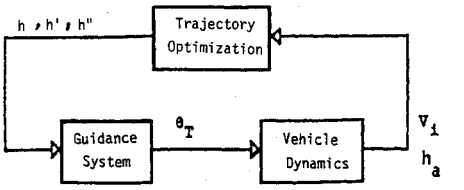

Fig. 5 Fully adaptive guidance system for initial phase.

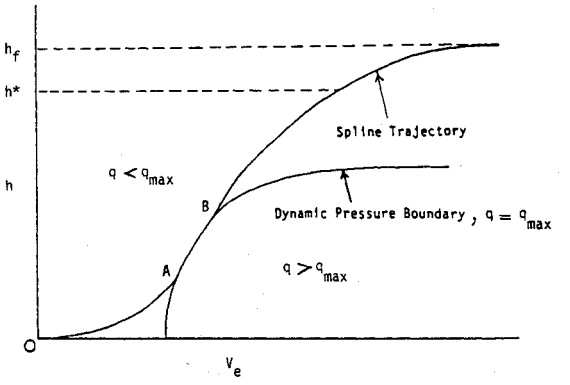

Fig. 6 Schematic illustration of flight path with dynamic pressure constraint.

parameters of the new spline trajectory originating at that point.

At time t'', the vehicle altitude h_a may once again exceed the error margin ϵ from the desired trajectory, which was generated at $t = t'$. Then, with the current values of h_a and h_a' as new initial conditions, a fresh two-segment cubic spline ascent profile is generated, and the one generated at $t = t'$ is discarded. The gimbal angle is recalculated to follow this path. This process is continued until the vehicle reaches the altitude h^*. This fully adaptive guidance scheme concept is illustrated in Fig. 4, and the schematic block diagram is presented in Fig. 5.

The present fully adaptive guidance concept, in which the vehicle at each given instance follows a locally optimum path generated in real time, is well suited to handle the off-nominal system performance and variations in weather usually prominent at low and moderate altitudes. It exploits all of the favorable altitude dispersions. One disadvantage, however, is that it is computationally intensive because the entire problem is reworked whenever a new trajectory is generated. However, by a judicious choice of h^*, the computational requirements can be kept to a minimum.

Determination of θ_T

Consider the equilibrium of forces along and normal to inertial flight path (Fig. 3),

$$m\dot{V}_i = T\cos(\theta_T - \gamma_i) - mg\sin\gamma_i - L\sin(\gamma_e - \gamma_i) - D\cos(\gamma_e - \gamma_i) \tag{13}$$

$$mV_i\dot{\gamma}_i = T\sin(\theta_T - \gamma_i) - mg\cos\gamma_i + L\cos(\gamma_e - \gamma_i) - D\sin(\gamma_e - \gamma_i) \tag{14}$$

Here, L and D are aerodynamic lift and drag forces and are evaluated using the empirical aerodynamic model given in Appendix C.

The inertial flight-path angle γ_i for flight along the desired spline ascent profile is given by

$$\gamma_i = \sin^{-1}\left(\frac{h'\dot{V}_i}{V_i}\right) \tag{15}$$

so that

$$\dot{\gamma}_i = \frac{1}{V_i\cos\gamma_i}\left[(h''\dot{V}_i^2 + \ddot{V}_i h') - \frac{h'\dot{V}_i^2}{V_i}\right] \tag{16}$$

The dot ($\dot{}$) represents differentiation with respect to time. The quantities h' and h'' can be obtained by differentiating Eq. (8) with respect to inertial velocity V_i.

Equating the expressions for $\dot{\gamma}_i$ from Eqs. (14) and (16) and solving for θ_T, we get

$$\theta_T = \sin^{-1}\left\{\frac{m}{T}\left[\frac{1}{\cos\gamma_i}(h''\dot{V}_i^2 + \ddot{V}_i h') - \frac{h'\dot{V}_i^2}{V_i}\right] - \frac{L}{T}\cos(\gamma_e - \gamma_i) + \frac{D}{T}\sin(\gamma_e - \gamma_i) + \frac{mg}{T}\cos\gamma_i\right\} + \gamma_i \tag{17}$$

The acceleration along the inertial flight path is given by

$$\dot{V}_i = \frac{T}{m}\cos\left[\theta_T - \sin^{-1}\left\{\frac{h'\dot{V}_i}{V_i}\right\}\right] - \frac{gh'\dot{V}_i}{V_i} - \frac{L}{m}\sin(\gamma_e - \gamma_i) - \frac{D}{m}\cos(\gamma_e - \gamma_i) \tag{18}$$

The values of θ_T and $\dot{V}_i$ are to be determined by the solution of Eqs. (17) and (18). For simplicity, the higher-order derivative $\ddot{V}_i$, which has to be numerically evaluated, was ignored in the calculations.

Dynamic Pressure Constraint

When this constraint, as given by Eq. (7), becomes active, the following approach is taken:

1) Determine points A and B (Fig. 6), where the spline trajectory intersects the dynamic pressure boundary.

2) At point A, leave the spline trajectory and fly along path AB, sticking to the dynamic pressure boundary.

3) At point B, depart from the dynamic pressure boundary, return to the spline trajectory, and continue.

4) Points A and B of attachment and detachment with the dynamic pressure boundary depend on the shape of the spline profile, which in turn depends on h_1 and h_1'.

5) The sensitivity calculations in the gradient optimization of the spline profile are not performed for the flight segment AB because the dynamic pressure boundary is a fixed curve for the given value of q_{max}. However, the location of points A and B depends on h_1 and h_1', as mentioned above. In this manner, the dynamic pressure constraint is incorporated in the optimization process.

Equation of Flight Path AB

The constraint to be satisfied for flight along AB is

$$\tfrac{1}{2}\rho V_e^2 = q_{\max} \tag{19}$$

where $q_{\max}$ is the limiting dynamic pressure. With $\rho = \rho_0 e^{\beta h}$, $\beta = -0.0000347$,

$$h = \frac{1}{\beta} \ell n \left(\frac{2q_{\max}}{\rho_0 V_e^2} \right) \tag{20}$$

$V_e = \sqrt{(V_i \cos\gamma_i - V_0)^2 + (h' V_i)^2}$, where $V_0 = \Omega R_e \cos\lambda$, the tangential velocity on the Earth's surface.

For simplicity, we assume that the flight-path angle γ_i varies slowly along AB so that γ_i can be assumed constant, say, equal to γ_{ic}. Such an assumption avoids time-consuming computations of derivatives of γ_i.

Then,

$$h' = -\frac{\rho}{\beta q_{\max}} \left[(V_i \cos\gamma_i - V_0) \cos\gamma_i + V_i \sin^2\gamma_{ic} \right] \tag{21}$$

$$\dot{V}_i = \frac{V_i \sin\gamma_{ic}}{h'} \tag{22}$$

$$\gamma_e = \sin^{-1}\left(\frac{V_i \sin\gamma_{ic}}{V_e} \right) \tag{23}$$

$$\theta_T = \cos^{-1} \times \left[\frac{m\dot{V}_i + D\cos(\gamma_e - \gamma_{ic}) + L\sin(\gamma_e - \gamma_{ic}) + mg\sin\gamma_{ic}}{T} \right] + \gamma_{ic} \tag{24}$$

and

$$T = \frac{D\sin(\gamma_e - \gamma_{ic}) - L\cos(\gamma_e - \gamma_{ic}) + mg\cos\gamma_{ic}}{\sin(\theta_T - \gamma_{ic})} \tag{25}$$

Equations (24) and (25) give the control angle and thrust variation for flight along the dynamic pressure boundary, $q = q_{\max}$.

Terminal Phase

This phase extends from altitude of h^* to LEO. The altitude h^* can be chosen so that the vehicle is virtually out of the Earth's atmosphere in the terminal phase. The terminal phase is assumed to consist of a single spline segment, and the only free parameter $h^{*\prime}$ is determined by the gradient optimization technique as before. This single-segment spline profile forms the nominal path for the terminal phase, and a proportional plus derivative feedback control is employed to determine the correction to the gimbal angle as follows:

$$\Delta\theta_T = K_1(h_a - h_{\text{des}}) + K_2(h_a' - h_{\text{des}}') \tag{26}$$

Here K_1 and K_2 are feedback gain parameters and are held constant. A block diagram of this control scheme is presented in Fig. 7. This approach, with constant gains, is computationally efficient but requires that deviations from the nominal path be small. Therefore, it is well suited for the terminal phase because aerodynamic forces are negligibly small compared to the thrust force. A disadvantage of the approach is that constant gains cannot always insure optimal performance.

Application

The adaptive guidance scheme developed earlier was applied to the problem of a generic, aero-assisted rocket booster for an equatorial launch ($L = \lambda = 0$) to LEO. The assumed terminal conditions at the Hohmann transfer orbit are: $V_f = 26{,}000$ ft/s, $h_f = 400{,}000$ ft, and $h_f' = 0$.

The vehicle is assumed to have the following characteristics:

Initial weight	= 800,000 lb
Thrust	= 1 million lb
Specific impulse	= 450 s
Height	= 100 ft
Diameter	= 14 ft
Semiapex angle	= 15 deg
Wingspan	= 42 ft
Wing root chord	= 75 ft
Wing area	= 1400 ft^2

(27)

A schematic sketch of the vehicle is presented in Fig. 8. The aerodynamic forces on the boost vehicle are evaluated using the empirical model given in Appendix C. The angle of attack is assumed to be held constant at some chosen value throughout the ascent to LEO. The thrust is assumed to be held constant at the value of 1 million lb listed here, except during flight along the dynamic pressure constraint, where throttling down to a lower value, as given by Eq. (25) may be necessary. The thrust is assumed to be restored to its full value on leaving the dynamic pressure boundary.

The excursions of gimbal angles are assumed to be limited to $\theta_{T\max} = 74.5$ deg and $\theta_{T\min} = -11.5$ deg. The limiting dynamic pressure ($q_{\max}$) is assumed equal to 575 lb/ft^2, which is the value used for the Space Shuttle.[5] In the case of the Space Shuttle, the dynamic pressure and angle-of-attack limitations are expressed as a single $q-\alpha$ constraint. However, such a specific approach is not taken here because the booster vehicle of the present study has a more generic nature. The values of $\epsilon = 0.01$ and $h^* = 200{,}000$ ft were used in the adaptive guidance scheme of the initial phase. The step sizes Δh_1, $\Delta h_1'$ [Eqs. (B3), Appendix B] were chosen equal to 5000 ft and 5.0 s, respec-

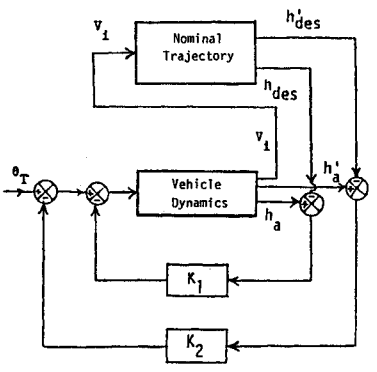

Fig. 7 Linear feedback control for terminal phase.

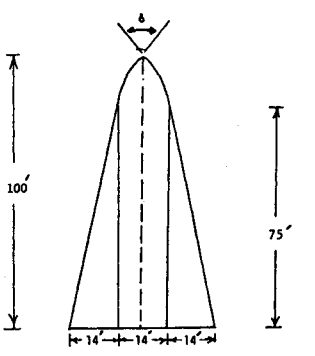

Fig. 8 Generic aero-assisted booster vehicle.

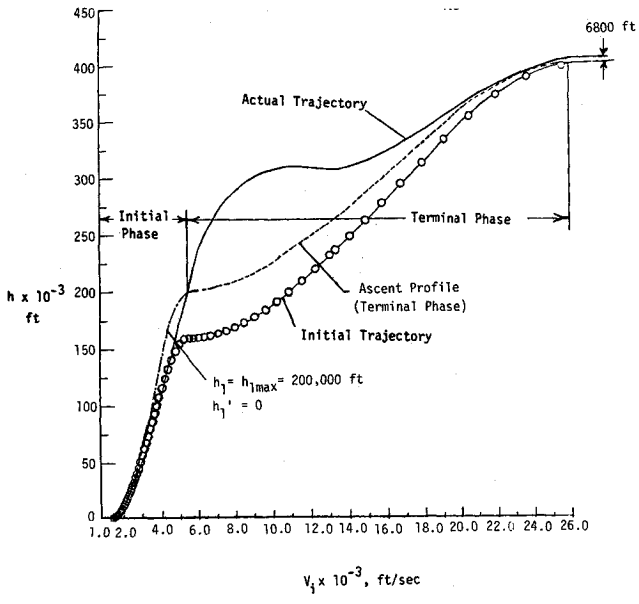

Fig. 9 Flight path of booster vehicle to LEO; $\alpha = 2$ deg.

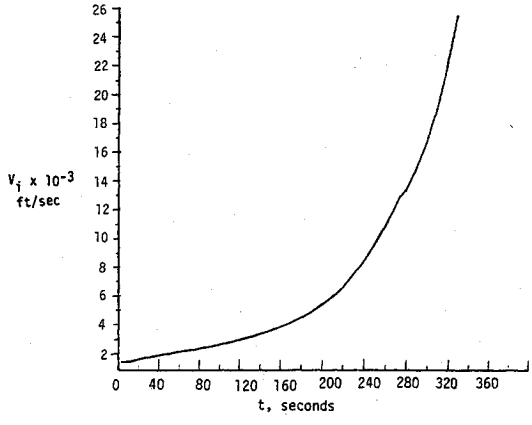

Fig. 10 Variation of inertial velocity with time.

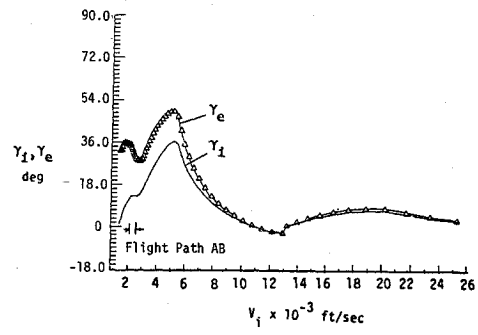

Fig. 11 Variation of flight-path angles with inertial velocity.

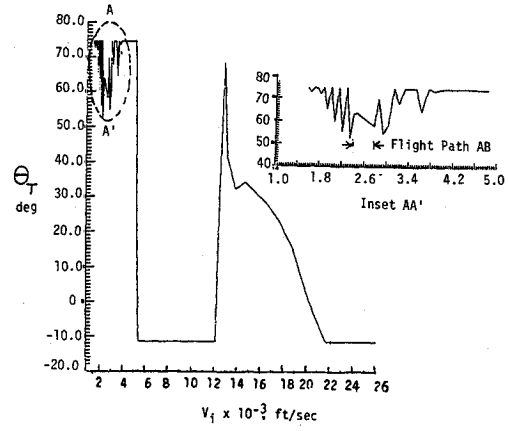

Fig. 12 Variation of gimbal angle with inertial velocity.

tively. When h_1 and h_1' were unconstrained and were allowed to assume any values as dictated by gradient algorithm, the trajectory in the terminal phase came out as one consisting of an overshoot above h_f, followed by a descent. To avoid loss of altitude, the h_1' parameter was further constrained as $h_1' > 0$, and h_1 was limited to some maximum value. Bringing in such additional constraints may result in suboptimal trajectories compared to the ones with unconstrained values of h_1 and h_1'. However, this process gives physically more realistic ascent profiles characteristic of flight paths to LEO.

Results and Discussion

Typical results of this study are presented in Figs. 9–15. From Fig. 9, we observe that the simulated booster vehicle moves close to the initial spline trajectory only up to 150,000 ft. This was true even though several profiles were generated at various times. All of these profiles are contained in the envelope formed by the initial profile and the one with limiting values of $h_1' = 0$ and $h_1 = h_{1max}$. Subsequently, the actual flight path of the simulated vehicle deviates considerably. Such differences arise even when the same density model is used in both the simulation of vehicle dynamics and derivation of ascent profile. Therefore, the normal acceleration term $V_i\dot{\gamma}_i$, which is ignored in the derivation of optimal ascent profile (Appendix B) but considered in the simulation of vehicle dynamics, appears to be the reason for these differences. For better agreement, the normal acceleration term should be considered in spline optimization which, however, was not attempted here.

The values of $h_1 = 160{,}000$ ft and $h_1' = 0$ were obtained for the optimal trajectory generated at $t = 0$. As the vehicle moved along, the values of h_1 increased for subsequent optimal trajectories. However, for the reasons mentioned earlier, the value of h_1 was frozen at $h_1 = 200{,}000$ ft. In general, $h_1 \neq h^*$. The gradient optimization algorithm occasionally moved back and forth because of numerical errors. The calculations were stopped when the object function showed a decreasing trend from the previous iteration by a predetermined accuracy ($\pm 10^{-4}$).

The velocity of the booster with respect to the inertial frame of reference increases rapidly (Fig. 10), with flight-path accelerations approaching 10 g. In this study, no constraint was imposed on flight-path acceleration. The value of the gain parameters K_1 and K_2, which gave good stability and minimum error of +6800 ft in final altitude, were found to be $K_1 = -5 \times 10^{-5}$ and $K_2 = -0.175$. This error in final altitude can be further minimized by using more sophisticated techniques of optimal control theory.

The flight-path angles γ_i and γ_e (Fig. 11) reach their maximum values around $V_i = 5500$ ft/s. For higher velocities, both approach zero on account of the imposed condition $h_f' = 0$. The gimbal angle variation is shown in Fig. 12, where the inset gives a blowup of the θ_T variation up to $V_i = 5000$ ft/s. The gimbal angle quite often hits the upper limit of 74.5 deg in the early part of flight. For velocities ranging approximately from 5500 to 12,500 ft/s, the altitude of the simulated vehicle is much higher than the corresponding value for the nominal path in terminal phase (Fig. 9). To counter this, the gimbal angle remains at its lower limit of −11.5 deg. Subsequently,

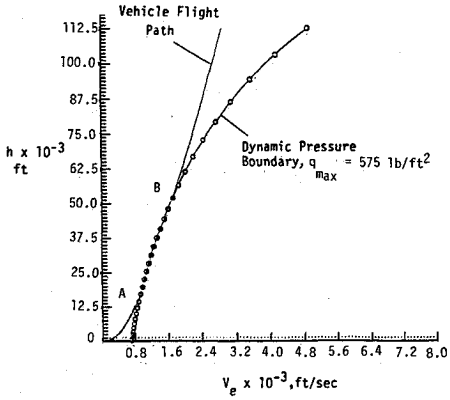

Fig. 13 Flight path with dynamic pressure constraint.

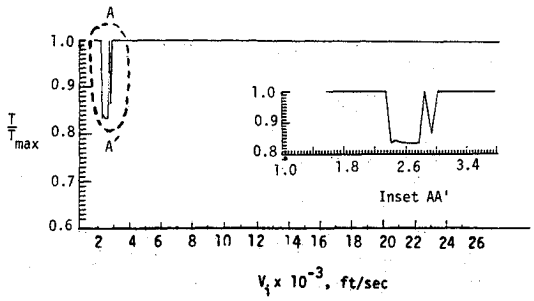

Fig. 14 Variation of thrust with inertial velocity.

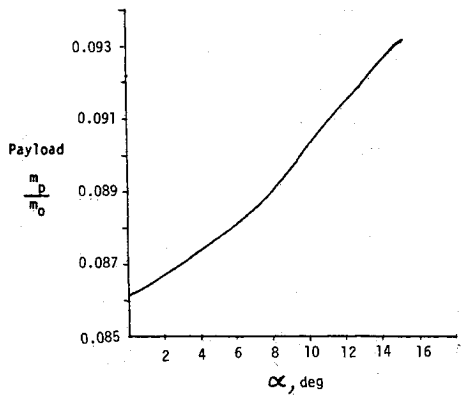

Fig. 15 Variation of payload with angle of attack.

when the altitude differences reduce, the gimbal angle assumes positive values. Eventually, it comes back to its lower limit as orbital velocity is reached on account of the condition $h_f' = 0$.

The portion of flight path AB along the dynamic pressure boundary is shown in Fig. 13. The approximation that the flight-path angle γ_i is constant along this path actually results in a $\pm 5\%$ variation in dynamic pressure from q_{max} along path AB. The gimbal angle varies smoothly for this portion of flight, as shown in Fig. 12. The thrust is throttled down to about 82% of the maximum value for flight path AB (Fig. 14). Although a continuous variation in thrust was assumed along path AB, a step reduction to 82% of the maximum value on hitting the dynamic pressure limit appears to be a good practical approximation. The thrust is assumed to be restored to its full value as soon as $q < q_{max}$. On account of this, the vehicle may hit the q_{max} boundary for the second time, as shown in the inset of Fig. 12.

The final value of the mass ratio m_p/m_0 is a measure of the fraction of initial mass delivered as payload to LEO. Comparing the payloads with $\alpha = 2$ deg, the initial optimum spline trajectory indicated a value equal to 0.1214. However, the simulated vehicle actually gives a value of 0.08677. Further, the single-segment optimal path of the terminal phase indicated a value of 0.103. These differences are attibuted to the neglect of the normal acceleration term in spline optimization and to the introduction of other factors that lead to suboptimal performance.

With aero-assist capability, i.e., using aerodynamic lift of wings and the body, the payload ratio increases as shown in Fig. 15. For $\alpha = 15$ deg, an improvement of 7.25% is indicated when compared to the baseline case of no aero-assist.

Concluding Remarks

An adaptive guidance law based on cubic spline representation of the flight path to low Earth orbit and incorporating dynamic pressure constraint is presented. The parameters of the cubic spline functions are optimized for maximum payload to low Earth orbit. However, some additional constraints were introduced to insure physically meaningful solutions, which results in suboptimal performance compared to unconstrained cubic spline functions. Such an approach in which the form of ascent trajectory is specified may be slightly inferior to more rigorous methods based on the calculus of variations. But the present method has a definite advantage in that it is mathematically simpler and computationally efficient and is well suited for application to the problem of single-stage to low Earth orbit where the total time of flight is only a few minutes.

The proposed two-phase adaptive guidance scheme is designed to handle unexpected changes in launch conditions, off-nominal system performance, and variations in weather. However, such an exercise was not actually carried out.

Appendix A: Coordinate Systems and Transformation Matrices

Inertial System ($x_i y_i z_i$)

This system is fixed at the center of the Earth and does not rotate with Earth (Fig. 2). The x_i and y_i axes lie in the plane of the equator and oz_i points in the direction of Earth's spin vector. The ox_i axis is assumed to point at some fixed object chosen at the instance of launch.

Earth-Fixed System ($x_e y_e z_e$)

This system also has the origin at the center of the Earth, but it rotates with the Earth. At $t = 0$, the $x_e y_e z_e$ system is assumed to coincide with $x_i y_i z_i$ axes system.

Navigational System ($x_n y_n z_n$)

This axes system has the origin on the surface of the Earth and at the point of intersection of the surface of the Earth and the radius vector drawn from the center of the Earth to the booster. Such a frame of reference is useful in tracking and navigation. Note that this axes system is a moving system and, at any time, lies directly below the booster vehicle. The ox_n axis is assumed to point to the local north, oz_n toward the center of Earth, and oy_n downrange to the east.

Body-Fixed System ($x_b y_b z_b$)

This system is fixed to the body with the origin at its center of gravity. The ox_b axis is assumed to point in the direction of the inertial flight path, and oy_b to be perpendicular to ox_b and to the plane of symmetry of the vehicle, assuming that such a a plane exists. The oz_b axis lies in the plane of symmetry and is perpendicular to the $ox_b y_b$ plane.

The introduction of this axes system facilitates the description of vehicle position, velocity, and also the aerodynamic, propulsive, and control forces acting on the vehicle.

Transformation of Vectors

Various transformation matrices of the type C_i^j, from system i to system j, were determined using the procedure given in Ref. 6.

Position and Velocity of the Vehicle

Location of the booster vehicle with respect to Earth,

$$R_e = C_i^e R_i$$

latitude,

$$\Lambda = \sin^{-1}(z_e/|R|)$$

and longitude,

$$L_0 = \sin^{-1}\left(\frac{y_e}{|R|\cos\lambda}\right)$$

where

$$|R| = \sqrt{x_i^2 + y_i^2 + z_i^2}$$

Velocity vectors with respect to Earth and navigational axes systems can be obtained as follows. The boldface $\boldsymbol{V}$ is used to denote a three-dimensional velocity vector and to distinguish it from previously used V, which generally denotes the magnitude of velocity:

$$\boldsymbol{V}_e = \dot{C}_i^e R_i + C_i^e \boldsymbol{V}_i$$

$$\boldsymbol{V}_n = \dot{C}_i^n (R_i - R_{01}) + C_i^n (\boldsymbol{V}_i - \dot{R}_{01})$$

where R_{01} is the radius vector (expressed in the $x_i y_i z_i$ system) from Earth's center to the origin of the $x_n y_n z_n$ system (Fig. 2). The heading, bank, and pitch angles of the booster, as observed in the navigational coordinate system, can be obtained from the Euler angles between the $x_b y_b z_b$ and $x_n y_n z_n$ systems. In this paper, the SYSPAC routines described in Ref. 7 were used in directional cosine matrix and Euler angle computations.

In the preceding equations, various directional cosine matrices and their derivatives are to be continuously evaluated. This is done by using the procedure given in Ref. 6.

Appendix B: Gradient Optimization

The cost function is defined as

$$J = \frac{m_p}{m_0} \tag{B1}$$

with $m_p = m_0 - \dot{m}\int \mathrm{d}t$, and $\dot{m} = T/I_{sp}g$, and $\mathrm{d}t = \mathrm{d}V_i/\dot{V}_i$,

$$J = 1 - \left(\frac{T}{I_{sp} m_0 g}\right)\int_{V_0}^{V_f} \frac{\mathrm{d}V_i}{\dot{V}_i} \tag{B2}$$

where h_1 and h_1' are two parameters to be determined such that the cost function J is maximized. For this purpose, the iterative procedure is as follows.

1) Assume some suitable starting values of h_1 and h_1', designated as h_{10} and h_{10}'.

2) Obtain sensitivity coefficients $\partial J/\partial h_1$ and $\partial J/\partial h_1'$ (as given later) for the assumed values of h_{10} and h_{10}'.

3) Obtain new values of h_1 and h_1' using the following expressions,

$$h_1 = h_{10} + \Delta h_1 \ \text{SIGNUM}\left(\frac{\partial J}{\partial h_1}\right)$$

$$h_1' = h_{10}' + \Delta h_1' \ \text{SIGNUM}\left(\frac{\partial J}{\partial h_1'}\right) \tag{B3}$$

where Δh_1 and $\Delta h_1'$ are the suitable chosen incremental steps of h_1 and h_1'. The SIGNUM function is equal to $+1$ or -1, depending on whether the argument is positive or negative.

4) Repeat this process until a maximum value of J is obtained.

Sensitivity Coefficients with Respect to h_1

$$\frac{\partial J}{\partial h_1} = \frac{T}{I_{sp} m_0 g}\int_{V_0}^{V_f} \frac{1}{\dot{V}_i^2}\left(\frac{\partial \dot{V}_i}{\partial h_1}\right)\mathrm{d}V_i \tag{B4}$$

where

$$\frac{\partial \dot{V}_i}{\partial h_1} = \frac{\partial \dot{V}_i}{\partial \gamma_i}\frac{\partial \gamma_i}{\partial h_1} + \frac{\partial \dot{V}_i}{\partial \gamma_e}\frac{\partial \gamma_e}{\partial h_1} + \frac{\partial \dot{V}_i}{\partial \rho}\frac{\partial \rho}{\partial h_1} \tag{B5}$$

Using the equations of motion along and normal to flight path, we have

$$\dot{V}_i = \frac{1}{m}\left[T\cos(\theta_T - \gamma_i) - D\cos(\gamma_e - \gamma_i) - L\sin(\gamma_e - \gamma_i)\right] - g\sin\gamma_i \tag{B6}$$

and

$$\sin(\theta_T - \gamma_i) = \frac{m[V_i\dot{\gamma}_i + g\cos\gamma_i] + D\sin(\gamma_e - \gamma_i) - L\cos(\gamma_e - \gamma_i)}{T} \tag{B7}$$

where

$$\sin\gamma_i = \frac{h'\dot{V}_i}{V_i}, \qquad \sin\gamma_e = \frac{h'\dot{V}_i}{V_e}$$

and

$$V_e = \sqrt{(V_i\cos\gamma_i - V_0)^2 + (h'\dot{V}_i)^2}$$

In the following analysis, we ignore the normal acceleration term $V_i\dot{\gamma}_i$ with the assumption that the flight-path angle γ_i is a slowly changing, quasisteady variable, i.e., $\dot{\gamma}_i = 0$. Such an assumption may not be adequate, especially in the early stages of initial phase. However, it leads to much simpler and better-behaved expressions for various derivatives appearing in Eq. (B5). Then,

$$\frac{\partial \dot{V}}{\partial \gamma_i} = \frac{1}{m}\left[T\sin(\theta_T - \gamma_i)\left(1 - \frac{\partial \theta_T}{\partial \gamma_i}\right) - D\sin(\gamma_e - \gamma_i) + L\cos(\gamma_e - \gamma_i)\right] - g\cos\gamma_i \tag{B8}$$

$$\frac{\partial \dot{V}_i}{\partial \gamma_e} = \frac{1}{m}\left[-T\sin(\theta_T - \gamma_i)\frac{\partial \theta_T}{\partial \gamma_e} + D\sin(\gamma_e - \gamma_i) - L\cos(\gamma_e - \gamma_i)\right] \tag{B9}$$

$$\frac{\partial \dot{V}_i}{\partial \rho} = \frac{1}{m}\left[-T \sin(\theta_T - \gamma_i)\frac{\partial \theta_T}{\partial \rho} - \frac{D\cos(\gamma_e - \gamma_i) + L\sin(\gamma_e - \gamma_i)}{\rho}\right] \tag{B10}$$

$$\frac{\partial \theta_T}{\partial \gamma_i} = 1 - \frac{1}{T\cos(\theta_T - \gamma_i)} \times \left[mg\sin\gamma_i + D\cos(\gamma_e - \gamma_i) + L\sin(\gamma_e - \gamma_i)\right] \tag{B11}$$

$$\frac{\partial \theta_T}{\partial \gamma_e} = \frac{1}{T\cos(\theta_T - \gamma_i)}\left[D\cos(\gamma_e - \gamma_i) + L\sin(\gamma_e - \gamma_i)\right] \tag{B12}$$

$$\frac{\partial \theta_T}{\partial \rho} = \frac{1}{T\cos(\theta_T - \gamma_i)}\left[\frac{D\sin(\gamma_e - \gamma_i) - L\cos(\gamma_e - \gamma_i)}{\rho}\right] \tag{B13}$$

$$\frac{\partial \gamma_i}{\partial h_1} = \frac{1}{V_i \cos\gamma_i}\left[\dot{V}_i \frac{\partial h'}{\partial h_1} + h' \frac{\partial \dot{V}_i}{\partial h_1}\right] \tag{B14}$$

$$\frac{\partial \gamma_e}{\partial h_1} = \frac{1}{V_e^2 \cos\gamma_e}\left[V_e\left(\dot{V}_i \frac{\partial h'}{\partial h_1} + h' \frac{\partial \dot{V}_i}{\partial h_1}\right) - h'\dot{V}_i \frac{\partial V_e}{\partial h_1}\right] \tag{B15}$$

$$\frac{\partial V_e}{\partial h_1} = \frac{1}{V_e}\left(\dot{V}_i \frac{\partial h'}{\partial h_1} + h' \frac{\partial \dot{V}_i}{\partial h_1}\right)\left[h'\dot{V}_i - (V_i \cos\gamma_i - V_0)\tan\gamma_i\right] \tag{B16}$$

$$\frac{\partial \rho}{\partial h_1} = \rho\beta \frac{\partial h}{\partial h_1} \tag{B17}$$

Substituting Eqs. (B14–B17) in (B5), we get

$$\frac{\partial \dot{V}_i}{\partial h_1} = \frac{1}{\xi_1}\left[\left(A\frac{\partial \dot{V}_i}{\partial \gamma_i} + B\frac{\partial \dot{V}_i}{\partial \gamma_e}\right)\frac{\partial h'}{\partial h_1} + C\frac{\partial \dot{V}_i}{\partial \rho}\frac{\partial h}{\partial h_1}\right] \tag{B18}$$

where

$$A = \frac{\dot{V}_i}{V_i \cos\gamma_i} \tag{B19}$$

$$B = \frac{1}{V_e^2 \cos\gamma_e}\left[\dot{V}_i V_e - \left(\frac{h'\dot{V}_i^2}{V_e}\right)\left\{h'\dot{V}_i - \tan\gamma_i(V_i\cos\gamma_i - V_0)\right\}\right] \tag{B20}$$

$$C = \rho\beta \tag{B21}$$

$$\xi = 1 - h'\left(\frac{1}{V_i\cos\gamma_i}\frac{\partial \dot{V}_i}{\partial \gamma_i} + \frac{1}{V_e\cos\gamma_e}\frac{\partial \dot{V}_i}{\partial \gamma_e}\right) \tag{B22}$$

$$\xi_1 = \xi + \left(\frac{h'^2\dot{V}_i}{V_e^3\cos\gamma_e}\right)\left\{h'\dot{V}_i - \tan\gamma_i(V_i\cos\gamma_i - V_0)\right\}\frac{\partial \dot{V}_i}{\partial \gamma_e} \tag{B23}$$

Similarly, the sensitivity coefficient with respect to h_1' can be obtained as

$$\frac{\partial \dot{V}}{\partial h_1'} = \frac{1}{\xi_1}\left[\left(A\frac{\partial \dot{V}_i}{\partial \gamma_i} + B\frac{\partial \dot{V}}{\partial \gamma_e}\right)\frac{\partial h'}{\partial h_1'} + C\frac{\partial h}{\partial h_1'}\frac{\partial \dot{V}_i}{\partial \rho}\right] \tag{B24}$$

The derivatives $\partial h'/\partial h_1$ and $\partial h'/\partial h_1'$ are obtained from the equation of spline (8) as follows.

Segment 1

For $V_0 < V_i < V_1$ and $0 < h < h_1$,

$$\frac{\partial h}{\partial h_1} = \frac{(V_i - V_0)^2(3V_1 - 2V_i - V_0)}{(V_1 - V_0)^3} \tag{B25}$$

$$\frac{\partial h}{\partial h_1'} = (V_i - V_1)\left(\frac{V_i - V_0}{V_1 - V_0}\right)^2 \tag{B26}$$

$$\frac{\partial h'}{\partial h_1} = \frac{6(V_i - V_0)(V_1 - V_i)}{(V_1 - V_0)^3} \tag{B27}$$

$$\frac{\partial h'}{\partial h_1'} = \frac{(V_i - V_0)(3V_i - 2V_1 - V_0)}{(V_1 - V_0)} \tag{B28}$$

Segment 2

For $V_1 < V_i < V_f$ and $h_1 < h < h_f$,

$$\frac{\partial h}{\partial h_1} = 1 - 3\left[\frac{V_i - V_1}{V_f - V_1}\right]^2 + 2\left[\frac{V_i - V_1}{V_f - V_1}\right]^3 \tag{B29}$$

$$\frac{\partial h}{\partial h_1'} = (V_i - V_1) - 2(V_f - V_1)\left[\frac{V_i - V_1}{V_f - V_1}\right]^2 + (V_f - V_1)\left[\frac{V_i - V_1}{V_f - V_1}\right]^3 \tag{B30}$$

$$\frac{\partial h'}{\partial h_1} = \frac{6}{(V_f - V_1)}\left[\left(\frac{V_i - V_1}{V_f - V_1}\right)^2 - \left(\frac{V_i - V_1}{V_f - V_1}\right)\right] \tag{B31}$$

$$\frac{\partial h'}{\partial h_1'} = 1 - \left(\frac{V_i - V_1}{V_f - V_1}\right)\left[4 - 3\left(\frac{V_i - V_1}{V_f - V_1}\right)\right] \tag{B32}$$

Appendix C: Estimation of Aerodynamic Lift and Drag Forces on Booster Vehicle

Lift

Using the data of Ref. 8 for the booster configuration at small angles of attack,

Subsonic Speeds: $(M < 1)$

$$C_L = 0.035\alpha$$

Supersonic Speeds: $(1 < M < 5)$

$$C_L = 0.02\alpha$$

Hypersonic Speeds: $(M > 5)$

Here, we use the method given in Ref. 9 and calculate the contribution of each component, i.e., nose (C_{LN}), cylindrical aft body ($C_{L,\text{aft}}$), and wings (C_{LW}). Aerodynamic interference between various components is ignored.

$$\text{Total lift coefficient,} \quad C_L = C_{LN} + C_{L,\text{aft}} + C_{LW}$$

Then the lift force

$$L = \frac{1}{2}\rho V_e^2 S_W C_L$$

where S_W is the wing area.

Drag

We use the following empirical relation derived by curve-fitting the Space Shuttle data of Ref. 5,

$$D = \frac{1}{2}\rho V_e^2 C_1\left(\frac{m_0}{C_2}\right)^{2/3}$$

where m_0 = initial mass of the vehicle, C_1 and C_2 are empirical constants, $C_1 = 542.61$, and $C_2 = 57{,}772.0$.

Acknowledgment

Research for the first author was provided by the National Aeronautics and Space Administration under NASA Contract NAS1-17919.

References

[1]White, A. W., Powell, R. W., Naftel, J. C., and Philips, W. P., "Booster and Orbiter Configurations," *Astronautics and Aeronautics,* Vol. 23, June 1983, pp. 38–42.

[2]Jones, R. A., and Donaldson, C. D., "From Earth to Orbit in a Single Stage," *Aerospace America,* Vol. 27, Aug. 1987, pp. 32–34.

[3]Walberg, G. D., "A Review of Aeroassisted Orbit Transfer," AIAA Paper 82-1378, Aug. 1982.

[4]Taylor, L. W., Gracey, C., and Armstrong, C. D., "A Guidance-Motivated Sensitivity Analysis of an Aero-Assisted Boost Vehicle," *Proceedings of the AIAA Guidance, Navigation, and Control Conference,* AIAA, New York, 1986, pp. 420–428.

[5]Staff of Flight Analysis Branch, *STS-1 Operational Flight Profile,* Vol. III, *Ascent-Cycle 3,* NASA Johnson Space Flight Center, Houston, TX, Rept. JSC-14483, May 1980.

[6]Regan, F. J., *Re-Entry Vehicle Dynamics,* AIAA Education Series, AIAA, New York, 1984, Chap. 8.

[7]Taylor, L. W., Suit, W. T., and Mayo, M. H., "A Program to Form a Multidisciplinary Data Base and Analysis for Dynamic Systems," AIAA Paper 81-2087, June 1981.

[8]Harloff, G. J., and Petrie, S. L., "Preliminary Aerothermodynamic Design Method for Hypersonic Vehicles," AIAA Paper 87-2545, 1987.

[9]Truitt, R. W., *Hypersonic Aerodynamics,* Ronald, New York, 1959, Chap. 8.